JOURNAL OF MATERIALS SCIENCE 29 (1994) 384–388

A transmission-electron-microscopy study of a face-centred-cubic phase in an Al–Li–Cu–Mg–Zr alloy

W. SHUNCAI, L. CHUNZHI, Y. MINGGAO
Laboratory of Metal Physics, Institute of Aeronautical Materials, Beijing 100095, China

Icosahedral T_2 phases can form either by solid-state precipitation or during solidification in Al–Li–Cu–Mg alloys. The T_2 phase forming during solidification can transform to an R phase at high annealing temperatures. The T_2 phase forming by solid-state precipitation coexists with the Y phase, which has a face-centred cubic (f.c.c.) structure with lattice parameter $a \approx 2.0$ nm and can form microtwins with the twin plane of (1 1 1). The orientation relationships between the C phase and the T_2 phase are: $i\bar{5}$||Y⟨0 1 1⟩, Y⟨1 1 3⟩; $i\bar{3}$||Y⟨1 1 1⟩, Y⟨1 2 3⟩, Y⟨1 1 5⟩; Y⟨2 3 5⟩; i2||Y⟨0 1 1⟩, Y⟨1 1 1⟩, Y⟨1 1 2⟩, Y⟨1 1 3⟩, Y⟨1 1 5⟩.

1. Introduction

In Al–Li–Cu (–Mg) alloys, an icosahedral T_2 phase can form either by solid-state precipitation or during solidification [1–3]. In Al–Li–Cu alloys, the T_2 phase shows microtwins [2, 4] and can transform into a T_B phase with high-temperature treatment [5]. In Al–Li–Cu–Mg alloys, the T_2 phase can transform to an R phase for annealing over 500 °C [6, 7]. Up to now, the crystal phases of orthorhombic O [7], hexagonal Z and tetragonal C [8, 9] have been identified. Audier *et al.* [10] have found a possible f.c.c. Al_2LiMg-phase intergrowth with the C phase.

In the materials studied, the f.c.c. phase independently existed in the grain boundaries. The purpose of this paper is to further study the structure of the Y phase and the orientation relationship between the Y and T_2 phase; some interesting results were found.

2. Experimental procedure

The chemical compositions of the experimental alloy were 2.55 wt % Li, 1.29 wt % Cu, 0.93 wt % Mg, 0.13 wt % Zr and the balance was Al. The ingot was obtained by semi-continuous direct-chill casting, after homogenization at 520 °C for 20 h. The specimens were quenched in cold water and then aged at 190 °C for 12 h after solution heat treatment at 525 °C for 1 h. The specimens for observation by transmission electron microscopy (TEM) were prepared by two-jet electropolishing in an electrolyte containing one part of HNO_3 to three parts of CH_3OH (by volume). The TEM observation was performed on a H800 transmission electron microscope at 200 k V.

3. Results and discussions

3.1. The structure of the Y phase

A typical morphology of the Y phase in the aged condition is shown in Fig. 1. It can be seen that the Y phase is rather rough and exists in the grain boundary.

Fig. 2 is a series of selected area diffraction (SAD) patterns from the Y phase, rotating along the $[\bar{2}\,2\,0]^*$ axis from the [0 0 1] zone. The reflection conditions show the Y phase has a f.c.c. structure with lattice parameter $a = 2$ nm. Comparing practical tilting with calculated angles, as shown in Table I, further confirms the correctness of the structure determined.

3.2. The twins of the Y phase

The Y phase forms twins easily, Fig. 3 shows the SAD patterns of twins. Fig. 3a shows the following twin relationship: $(\bar{2}\,2\,0)_1 || (2\,\bar{2}\,0)_2$, $[1\,1\,0]_1 || [1\,1\,4]_2$. Fig. 3b shows the following twin relationship: $(\bar{2}\,2\,0)_1 || (2\,\bar{2}\,0)_2$, $[1\,1\,\bar{1}]_1 || [\bar{1}\,\bar{1}\,5]_2$. Fig. 3c shows the following twin relationship: $(1\,\bar{1}\,1)_1 || (\bar{1}\,5\,\bar{1})_2$, $[5\,3\,\bar{2}]_1 || [\bar{1}\,1\,6]_2$. Fig. 3d shows the following twin relationship: $(1\,1\,1)_1 || (1\,1\,1)_2$, $[\bar{1}\,0\,1]_1 || [1\,0\,\bar{1}]_2$.

The transformation matrix describing the above orientation relationships is

$$T = \tfrac{1}{3}\begin{bmatrix} -1 & 2 & 2 \\ 2 & -1 & 2 \\ 2 & 2 & -1 \end{bmatrix}$$

This matrix also describes the twin-orientation relationship in f.c.c. structures. The twins must be smaller than 1 nm and should be microtwins.

3.3. The relationship between the Y phase and T_2 phase

It should be recalled that the T_2 phase can form either by solid-state precipitation or during solidification [1–3]. The T_2 phase forming by solidification is larger than 1 μm and can transform to the R phase which exists both in grains and at grain boundaries in

0022–2461

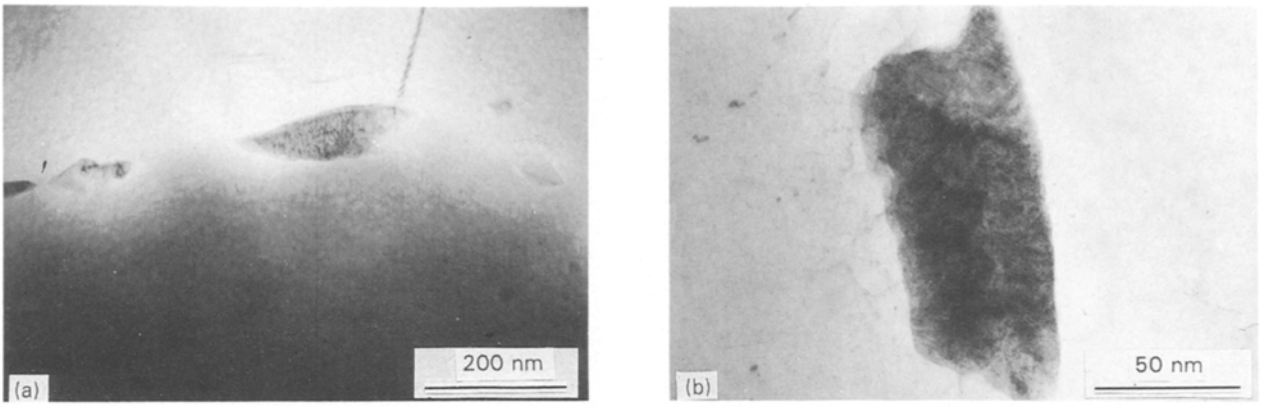

Figure 1 The morphologies of the Y phase in the grain boundary.

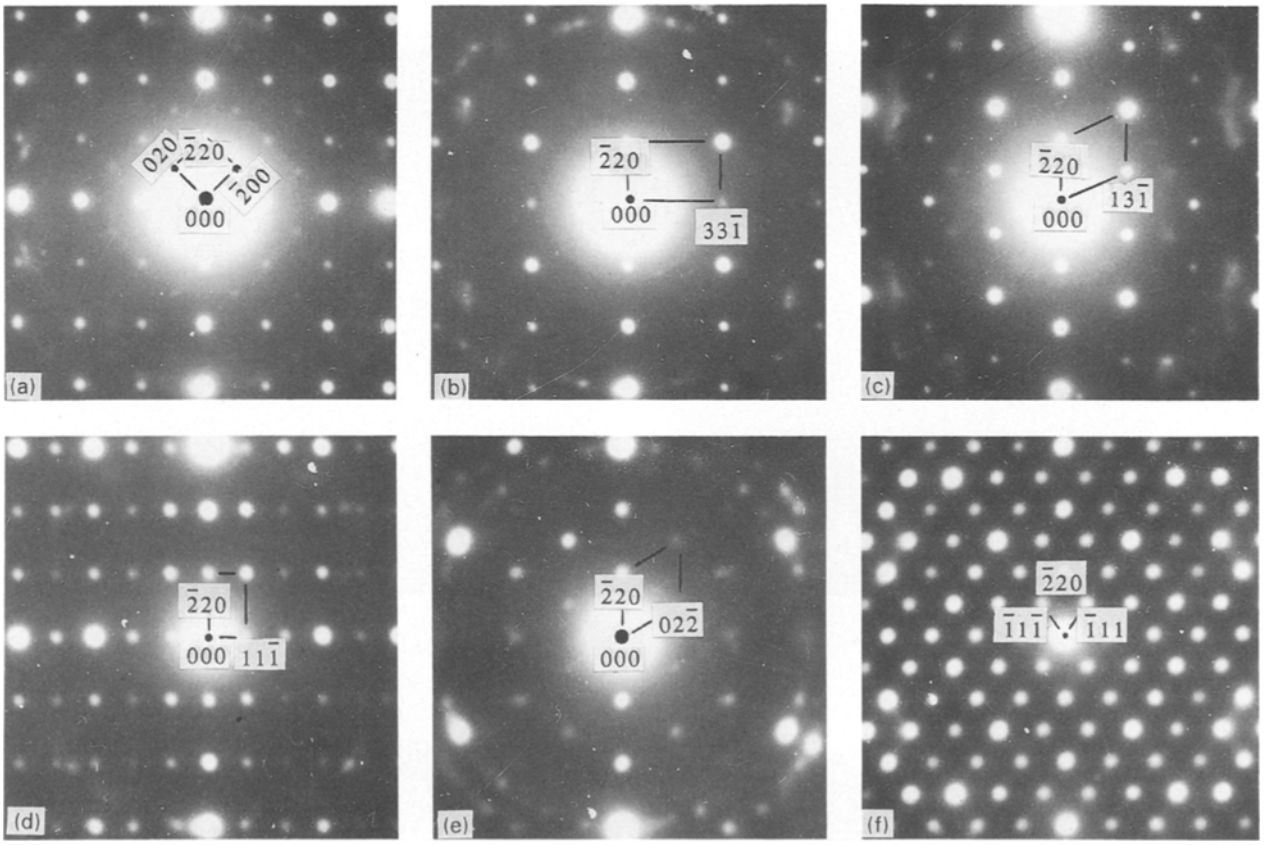

Figure 2 A series of SAD patterns along the $[\bar{2}20]^*$ axis from [001] zones: (a) [001], (b) [116], (c) [114], (d) [112], (e) [111], and (f) [110].

TABLE I The experimental and calculated angles (in degrees) included between [001] and other zones

Angles (deg)	Zones				
	[116]	[114]	[112]	[111]	[110]
Practical tilting angles	13	20	35	55	90
Calculated angles	13.3	19.5	35.3	54.7	90

annealing over 500 °C [6, 7]. The T_2 phase forming by solid-state precipitation is smaller than 0.2 μm and exists only in grain boundaries in the conventional aged treatment. In this case, the Y phase has the same morphology as the T_2 phase and the two phases coexist.

Fig. 4a shows the SAD pattern along the $\bar{5}$ axis of the T_2 phase. Ten-member-strong spots of three rings are clearly seen. The interplanar spacings corresponding to the first, second, and third rings are 0.377, 0.233 and 0.144 nm, respectively.

Fig. 4b shows the SAD pattern along the [0 1 1] axis of the crystal Y phase. The indexes of the ten-strong spots on the first ring are $3\bar{3}3$, $5\bar{1}1$, $51\bar{1}$, $33\bar{3}$, $04\bar{4}$, $\bar{3}3\bar{3}$, $\bar{5}1\bar{1}$, $\bar{5}\bar{1}1$, $\bar{3}\bar{3}3$, and $0\bar{4}4$; and their interplanar spacings are 0.385, 0.385, 0.385, 0.385, 0.354, 0.385, 0.385, 0.385, 0.385, and 0.354 nm, respectively. The indexes of the ten-strong spots on the second ring are $55\bar{5}$, $8\bar{2}2$, $82\bar{2}$, $55\bar{5}$, $06\bar{6}$, $\bar{5}5\bar{5}$, $\bar{8}2\bar{2}$, $\bar{8}\bar{2}2$, $\bar{5}\bar{5}5$, and

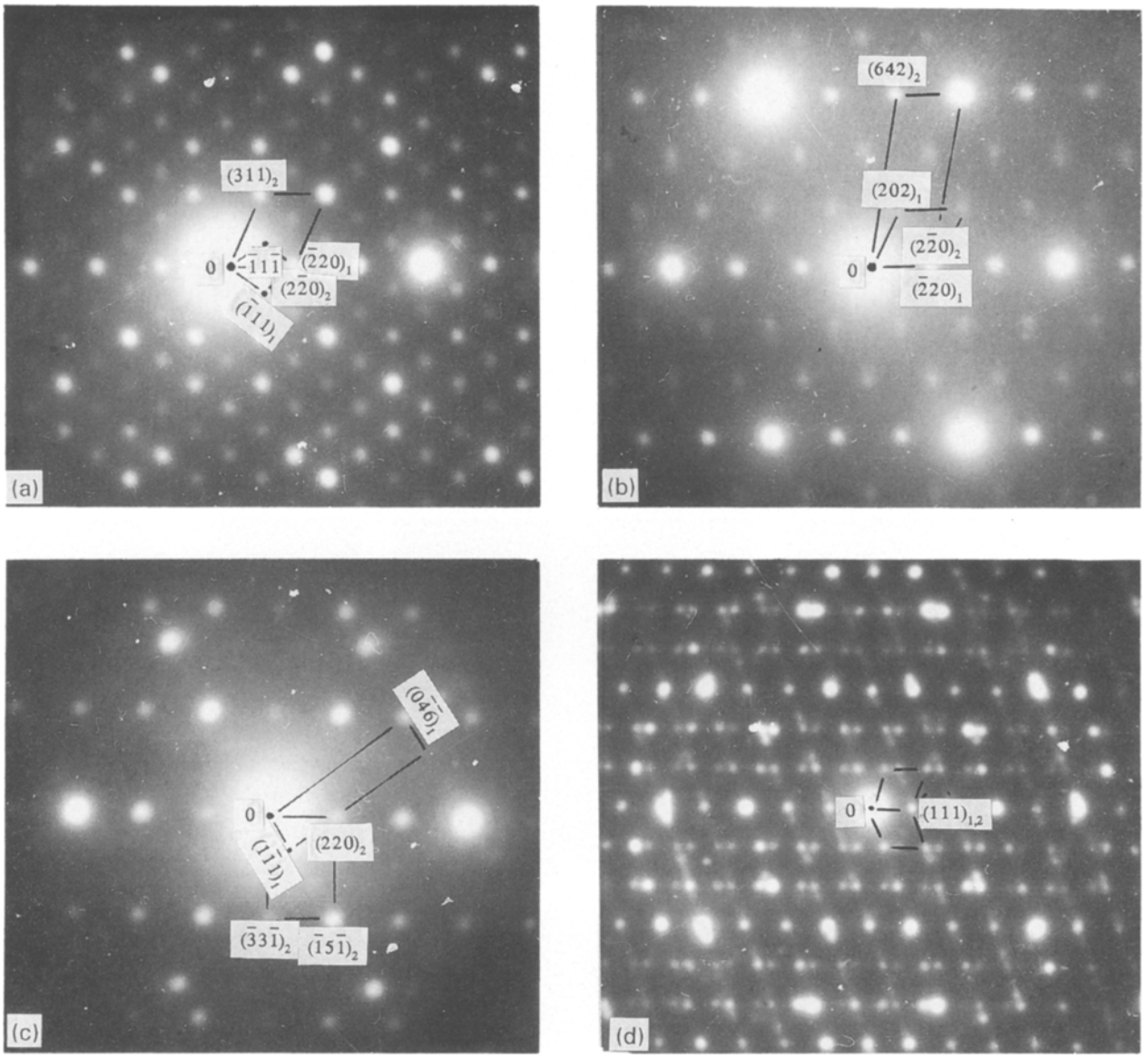

Figure 3 The SAD patterns from microtwins in the Y phase (a) $(\bar{2}\,2\,0)_1 \| (2\,\bar{2}\,0)_2$, $[1\,1\,0]_1 \| [1\,1\,4]_2$; (b) $(\bar{2}\,2\,0)_1 \| (2\,\bar{2}\,0)_2$, $[1\,1\,\bar{1}]_1 \| [\bar{1}\,\bar{1}\,5]_2$; (c) $(1\,\bar{1}\,1)_1 \| (\bar{1}\,5\,\bar{1})_2$, $[5\,3\,\bar{2}]_1 \| [\bar{1}\,1\,6]_2$; and (d) $(1\,1\,1)_1 \| (1\,1\,1)_2$, $[\bar{1}\,0\,1]_1 \| [1\,0\,\bar{1}]_2$.

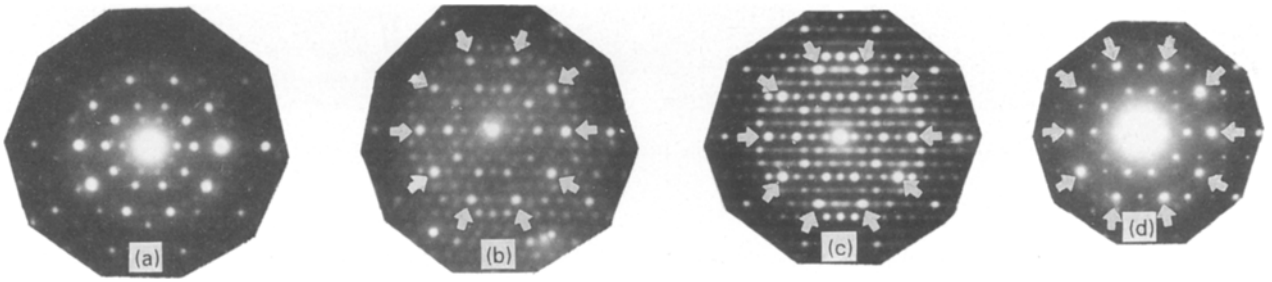

Figure 4 The SAD patterns from the T_2 and Y phase: (a) $\bar{5}$-axis SAD pattern of the T_2 phase; (b) and (c) [0 1 1] of the Y phase showing pseudo five-fold symmetries, and (d) [1 1 3] and corresponding [1 1 0] microtwin of the Y phase showing pseudo five-fold symmetry.

$0\,\bar{6}\,6$; and their interplanar spacings are 0.231, 0.236, 0.236, 0.236, 0.236, 0.231, 0.236, 0.236, 0.236, and 0.236 nm, respectively. The indexes of the ten-strong spots on the third ring are $8\,\bar{8}\,8$, $1\,3\,\bar{3}\,3$, $1\,3\,3\,\bar{3}$, $8\,8\,\bar{8}$, $0\,1\,0\,\bar{1}\,\bar{0}$, $\bar{8}\,8\,\bar{8}$, $\bar{1}\,\bar{3}\,3\,\bar{3}$, $\bar{1}\,\bar{3}\,\bar{3}\,3$, $\bar{8}\,\bar{8}\,8$, and $0\,\bar{1}\,\bar{0}\,1\,0$; and their interplanar spacings are 0.144, 0.146, 0.146, 0.144, 0.141, 0.144, 0.146, 0.146, 0.144, and 0.141 nm, respectively.

Fig. 4c shows the SAD pattern along the [0 1 1] axis of the Y phase, where the ten-member-strong spots of three rings are clearly seen; similar to Fig. 4b. It can also be clearly seen that some weak spots are blurred, which may be caused by twins compared with Fig. 3d.

Fig. 4d shows a [1 1 3] SAD pattern from the Y phase and a [1 1 0] SAD pattern from the twin. The indexes of the ten-strong spots on the first ring are $\bar{4}\,4\,0$, $\bar{3}\,3\,3$, $\bar{4}\,\bar{2}\,2$, $\bar{2}\,\bar{4}\,2$, $3\,\bar{3}\,3$, $4\,\bar{4}\,0$, $3\,\bar{3}\,\bar{3}$, $4\,2\,\bar{2}$, $2\,4\,\bar{2}$, and $\bar{3}\,3\,\bar{3}$; and their interplanar spacings are 0.354, 0.385, 0.408, 0.408, 0.385, 0.354, 0.385, 0.408, 0.408, and 0.385 nm, respectively. The indexes of the ten-strong

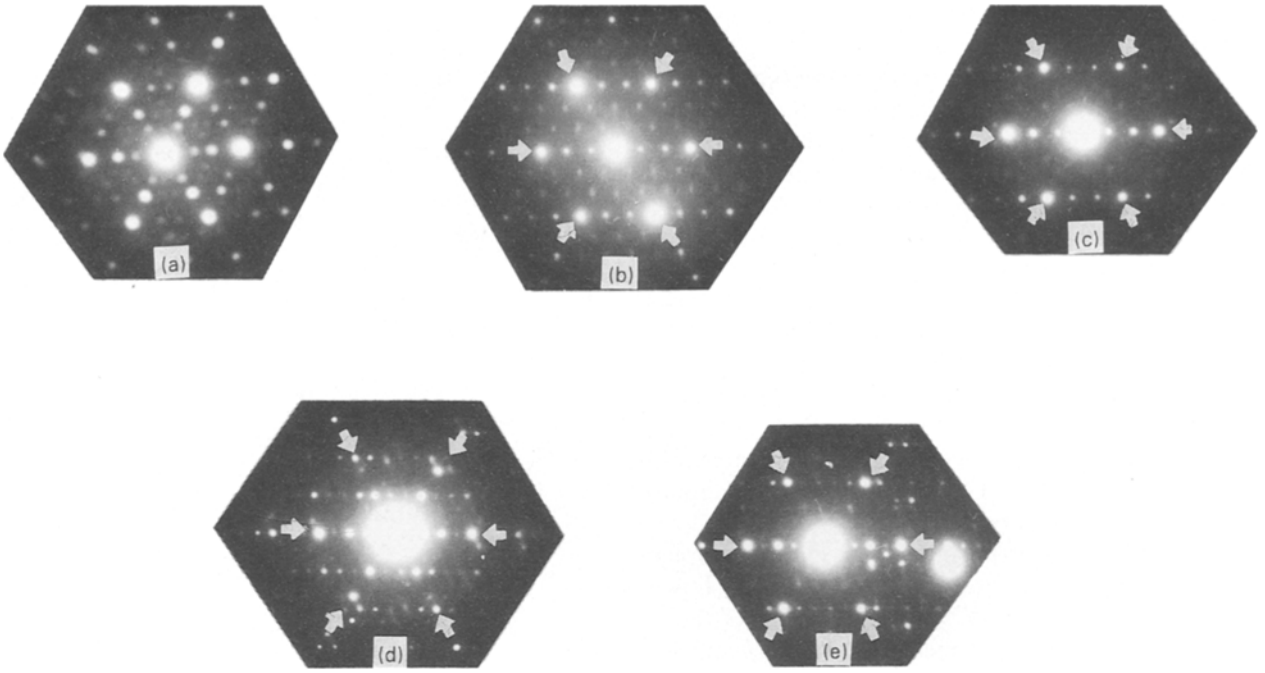

Figure 5 The SAD patterns from the T_2 and Y phases, (a) $\bar{3}$-axis SAD pattern from the T_2 phase; (b) to (e) are [1 1 1], [1 1 5], [1 2 3], [2 3 5], respectively, of the Y phase showing pseudo five-fold symmetries.

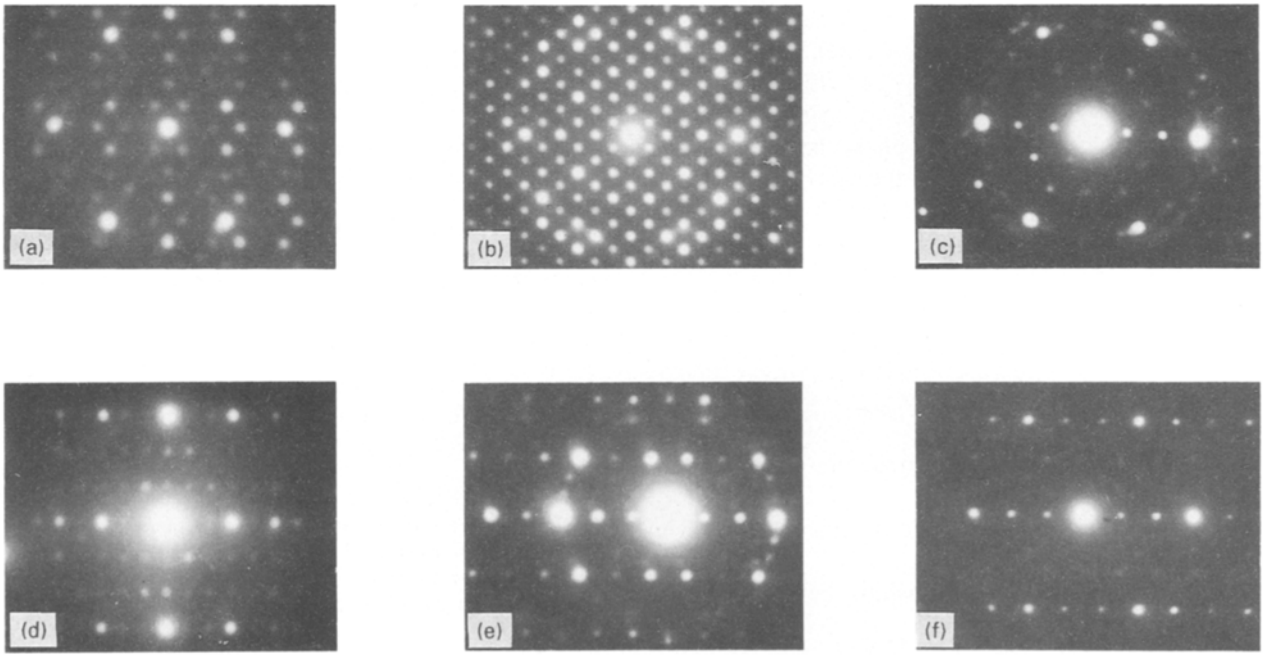

Figure 6 The SAD patterns from the T_2 and Y phases, (a) 2-axis SAD pattern from the T_2 phase; (b), (c), (d), (e), and (f) are [0 1 1], [1 1 1], [1 1 2], [1 1 3], [1 1 5], respectively, of the Y phase showing pseudo two-fold symmetries.

spots on the second ring are $\bar{6}60$, $\bar{5}55$, $22\bar{8}$, $\bar{2}2\bar{8}$, $55\bar{5}$, $66\bar{0}$, $55\bar{5}$, $22\bar{8}$, $\bar{2}2\bar{8}$, and $\bar{5}5\bar{5}$; and their interplanar spacings are 0.236, 0.231, 0.236, 0.236, 0.231, 0.236, 0.231, 0.236, 0.236, and 0.231 nm, respectively. Comparing fig. 4a and 4b–d, it is a coincidence that the second rings are more intense than the first and third rings.

Fig. 5a shows the SAD pattern along the $\bar{3}$ axis of the T_2 phase, in which six-strong-spot discs are clearly seen. The interplanar spacing corresponding to the ten-member-strong-spot rings is 0.233 nm. Fig. 5b shows the SAD pattern along the [1 1 1] axis of the crystal Y phase. The indexes of the six-strong-spots are $\bar{6}60$, $\bar{6}06$, $0\bar{6}6$, $6\bar{6}0$, $60\bar{6}$, and $0\bar{6}6$; and each of their interplanar spacings is 0.236 nm. Fig. 5c shows the SAD pattern along the [1 1 5] axis of the Y phase. The indexes of the six-strong-spots are $\bar{6}60$, $\bar{8}\bar{2}2$, $\bar{2}\bar{8}2$, $6\bar{6}0$, $82\bar{2}$, $28\bar{2}$; and each of their interplanar spacings is 0.236 nm. Fig. 5d shows the SAD pattern along the [1 2 3] axis of the Y phase. The indexes of the six-strong-spots on the first ring are $33\bar{3}$, $\bar{2}4\bar{2}$, $\bar{5}11$, $\bar{3}\bar{3}3$, $24\bar{2}$ and $5\bar{1}\bar{1}$; and their interplanar spacings are 0.385, 0.408, 0.385, 0.385, 0.408, and 0.385 nm, respectively. The indexes of the six-strong spots on the second

ring are $5\,5\,\bar{5}$, $\bar{4}\,8\,\bar{4}$, $\bar{9}\,3\,1$, $\bar{5}\,\bar{5}\,5$, $4\,\bar{8}\,4$, and $9\,\bar{3}\,\bar{1}$; and their interplanar spacings are 0.236, 0.204, 0.210, 0.236, 0.204, and 0.210 nm, respectively.

Fig. 5e shows the SAD pattern along the [2 3 5] axis of the Y phase. The indexes of the six-strong spots are $5\,5\,\bar{5}$, $\bar{3}\,7\,\bar{3}$, $\bar{8}\,2\,2$, $\bar{5}\,\bar{5}\,5$, $3\,\bar{7}\,3$ and $8\,\bar{2}\,\bar{2}$; and their interplanar spacings are 0.236, 0.244, 0.236, 0.236, 0.244, and 0.236 nm, respectively.

Fig. 6a shows the SAD pattern along the 2 axis of the T_2 phase. Fig. 6b–e shows the two-fold symmetries of the SAD patterns along the [0 1 1], [1 1 1], [1 1 2], [1 1 3], and [1 1 5] axes of the Y phase. Consequently, the ⟨0 1 1⟩ and ⟨1 1 3⟩ zones of the Y phase show pseudo five-fold symmetries; the ⟨1 1 1⟩, ⟨1 2 3⟩, ⟨1 1 5⟩, and ⟨2 3 5⟩ zones show pseudo three-fold symmetries; ⟨1 1 0⟩, ⟨1 1 1⟩, ⟨1 1 2⟩, ⟨1 1 5⟩ zones show psuedo two-fold symmetries.

Fig. 7 shows a superposition of the $i\bar{5}$ stereographic projection of the T_2 phase ($\bar{5}$, $\bar{3}$, and 2 poles are shown as solid shapes) on the Y [1 1 0] projection of the Y phase (poles are shown as open circles) with i2 coincidence on [1 1 0]. The deviation is, in general, less than 5°. The indexes in Fig. 7 have good coincidence, except those in italics, between the icosahedral phase ($Ti_{1-x}V_x$) and the f.c.c. crystalline phase ($NiTi_2$), which was observed directly by Zhang and Guo [11]. To sum up, the orientation relationship in Fig. 7 has: $i\bar{5}$||Y⟨0 1 1⟩ (three), and Y⟨1 1 3⟩ (three); $i\bar{3}$||Y⟨1 1 1⟩ (one), Y⟨1 2 3⟩ (four), Y⟨1 1 5⟩ (three), and Y⟨2 3 5⟩ (two); i2||Y⟨0 1 1⟩ (four), Y⟨1 1 1⟩ (five), Y⟨1 1 2⟩ (three), Y⟨1 1 3⟩ (two), and Y⟨1 1 5⟩ (six).

The T_2 phase and the Y phase have the same morphologies, which coexist in the same grain boundary. Besides, the Y phase can form microtwins (as here), and the T_2 phase can also form microtwins [2, 4]. All this strongly suggests that there are transformation relationships between the T_2 and the Y phase.

4. Conclusions

1. The Y phase has a f.c.c. structure with a lattice parameter $a = 2$ nm.

2. The Y phase can form microtwins with the twin plane of (1 1 1).

3. The orientation relationships between the Y phase and the T_2 phase are:
$i\bar{5}$||Y⟨0 1 1⟩, and Y⟨1 1 3⟩; $i\bar{3}$||Y⟨1 1 1⟩, Y⟨1 2 3⟩, Y⟨1 1 5⟩, and Y⟨2 3 5⟩; and $i\bar{2}$||Y⟨0 1 1⟩, Y⟨1 1 1⟩, Y⟨1 1 2⟩, Y⟨1 1 3⟩, and Y⟨1 1 5⟩.

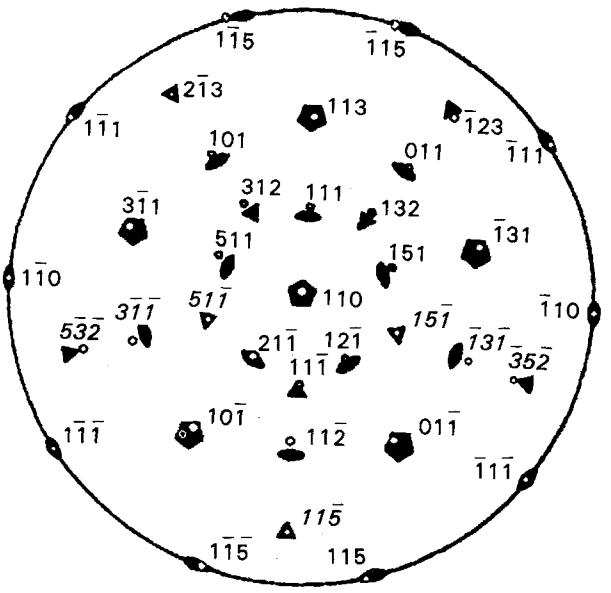

Figure 7 A stereographic projection of the T_2 and Y phases with $i\bar{5}$||Y[1 1 0]. The solid shapes are poles of the T_2 phase while the open circles are those of the Y phase.

References

1. H. K. HARDY and J. M. SILCOCK, *J. Inst. Met.*, **24** (1955) 523.
2. S. VECCHIO and D. M. WILLIAMS, *Met. Trans. A*, **19** (1988) 2875.
3. M. A. MARCUS and V. ELSER, *Phil. Mag. B*, **54(3)** (1986) L101–4.
4. M. H. TOSTEN, A. RAMANI, C. W. BARTGES, D. J. MICHEL, E. RYBA and P. R. HOWELL, *Scripta Metall.* **23** (1989) 829.
5. P. R. HOWELL, D. J. MICHEL and E. RYBA, *Scripa Metall.* **23** (1989) 825.
6. D. H. KIM and B. CANTOR, *J. Mater. Sci.* **23** (1988) 1695.
7. WANG SHUNCAI, LI CHUNZHI, WU YILEI, QIANG JUN and HAN YAFAN, *J. Mater. Sci. Lett.* **10** (1991) 643.
8. G. LAPASSET and A. LOISEAU, in "Proceedings of the Fourth International Al–Li Conference", edited by G. Champier *et al.* (J. de Physique, France, 1987) p. C3–489.
9. A. LOISEAU and G. LAPASSET, *Phil. Mag. Lett.* **57(5)** (1987) 165.
10. M. AUDIER, M. de BOISSIEU, C. JANOT and B. DUBOST, in "Proceedings of the Fifth International Al–Li Conference", edited by T. H. Sander Jnr, and E. A. Starke Jnr, Williamsburg, Virginia, March 27–31, 1989, p. 565.
11. Z. ZHANG and K. X. GUO, *Phil. Mag. B* **54(3)** (1986) L83.

Received 2 June
and accepted 17 November 1992